

# Structure and dynamics of interlayer species in a hydrated Zn-vermiculite. A molecular dynamics study

Mehdi Arab, Daniel Bougeard and Konstantin S. Smirnov\*

Laboratoire de Spectrochimie Infrarouge et Raman, UMR 8516 du CNRS, Bât. C5,  
Université des Sciences et Technologies de Lille, 59655, Villeneuve d'Ascq Cédex, France.  
E-mail: Konstantin.Smirnov@univ-lille1.fr

Received 13th January 2004, Accepted 27th February 2004  
First published as an Advance Article on the web 29th March 2004

The structure and dynamics of the interlayer species in hydrated Zn-vermiculite clay at 300 K were studied by means of molecular dynamics calculations. In a water-free structure, the  $\text{Zn}^{2+}$  ions adsorb on the surface of the clay layers. In the presence of  $\text{H}_2\text{O}$  molecules in the interlayer space  $\text{Zn}(\text{H}_2\text{O})_6^{2+}$  complexes are built under migration of the ions to the midplane of the interlayer space. The complexes are oriented in the interlayer space so that at least four water molecules interact *via* their H atoms with the O atoms of the clay surfaces. The calculations show that in the interlamellar space the Zn–water complexes have the same structure and internal dynamics as in aqueous solution. This dynamics was characterized in details on the basis of the calculations. The rotational motion of both the “bound” and “free” molecules proceeds mostly *via* a reorientation of the HH vector of the molecules. No exchange between the solvating water molecules and the “free” water of the interlayer space was observed in the time-scale of the calculations (2.4 ns). The residence time of the  $\text{H}_2\text{O}$  molecules in the second hydration sphere of the cations was computed to be approximately four times longer than in aqueous solution. This increase of the residence time corresponds to the decrease of the diffusion coefficient of the interlayer water, as compared to the molecules in the liquid. The single-particle dynamics of the non-solvating water molecules was studied by the analysis of the intermediate scattering functions and by calculation of the quasi-elastic neutron scattering spectra. The diffusion coefficients  $D = (0.91 \pm 0.11) \times 10^{-9} \text{ m}^2 \text{ s}^{-1}$  was obtained to be very close to that of the  $\text{H}_2\text{O}$  molecules in the uncharged clay.

## 1 Introduction

Clays are among the most abundant components of soils and play an important role in many industrial processes like catalysis, removal of contaminants from waste water, *etc.* All these processes are in relation with the layered structure of these aluminosilicates that also results in a large cation-exchange capacity of these compounds. The ability to accumulate and to exchange metallic cations makes the clays relevant for biogeochemical processes by driving the availability of the ions to biological substances. Zinc is after iron the second most abundant metallic cation in biological systems<sup>1</sup> and is also among the most phytotoxic elements after Al and Mn. Zinc cation is known to be very mobile<sup>2</sup> and a good knowledge of its complexation properties and of its dynamical behavior both in solutions and confined environments is of significant importance for understanding the underlying physico-chemical processes at the atomic level.

During the past decade, the molecular modeling was extensively used to study the swelling of the clay structures and the dependence of the swelling curves on the nature of the cationic species and on the content of water molecules in the interlamellar space.<sup>3–12</sup> These studies allowed to obtain a microscopic picture of the swelling process and to shed light on the structure of species present in the interlayer space of the hydrated clays. Less attention was, however, paid to the modelling of the dynamical behavior of the confined water and of cation–water complexes in the interlamellar space. For metallic cations in aqueous solution their structure-breaking/structure-forming properties, as well as the dynamical issues, were addressed in many modelling studies performed by both classical and quantum simulation techniques.<sup>13</sup> Structure and dynamics of solvated zinc(II) ion have already been studied

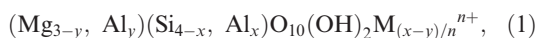
in a number of modelling studies.<sup>14–19</sup> However, to the best of our knowledge the behavior of the  $\text{Zn}^{2+}$  ions in hydrated clays have not been explored yet.

The present paper reports on the results of a molecular dynamics study of the structure and dynamics of water molecules and of  $\text{Zn}^{2+}$ –water complexes in the interlayer space of a vermiculite clay. This work is a continuation of our two recent articles on the structure and dynamics of water in a model uncharged structure of 2:1 clay<sup>12</sup> and on the structure and dynamics of  $\text{Zn}^{2+}$  ions in aqueous solution.<sup>19</sup> The results of these papers will therefore be used throughout the present article as reference data allowing to highlight the influence of the confinement and the presence of the counterions in the interlamellar space on the behavior of the interlayer species. Section 2 thoroughly describes the structural model of the Zn-vermiculite clay and reports details of the simulation procedure used. Section 3 deals with the results of the calculations and discusses the structure and the short-time dynamics of the interlayer species. The last part of the section deals with the diffusion of the species in the interlamellar space. Conclusions are summarized in Section 4.

## 2 Model and calculations

The structure of vermiculite used in the calculations is based on that determined by Mathieson.<sup>20</sup> The clay lattice belongs to the monoclinic  $C_c$  space group and has the parameters  $a = 5.33 \text{ \AA}$ ,  $b = 9.18 \text{ \AA}$ ,  $c = 28.90 \text{ \AA}$ , and  $\beta = 97.0^\circ$ .<sup>20</sup> The interlayer space consists of two interlayer voids and the repetition distance of the clay layers in the direction perpendicular to the clay surfaces ( $p$ -direction) is equal to

$d_{001} = c/2 \sin\beta$ . Vermiculite clays have the general chemical formula



where  $\text{M}^{n+}$  denotes a charge-balancing cation. The substitution of  $x$  silicon atoms in the tetrahedral sites and  $y$  magnesiums in the octahedral sites by aluminium atoms creates a charged structural unit (1) with the formal charge  $y-x$ . In reality, the atoms of the lattice do not bear the formal ionic charges and, therefore, the number of counterions  $\text{M}^{n+}$  necessary to compensate for the charge created by the substitution depends on the real charges on the atoms of the structure. Thus, a recent ONIOM study of 1:1 clay minerals resulted in a mean charge for oxygen atoms of  $-1.12 |e|$ , that is different from their formal ionic charge  $-2 |e|$ .<sup>21</sup> Semi-empirical calculations of cluster models of a montmorillonite clay with the use of the MNDO Hamiltonian showed a difference of  $0.5-0.6 |e|$  between the Mulliken charges of Si and Al atoms situated in the tetrahedral and octahedral sites, respectively.<sup>22,23</sup> Periodic Hartree-Fock calculations of zeolites and kaolinite clay structures showed that the charges of tetrahedrally coordinated silicon and aluminium atoms differ from each other by  $0.2-0.4 |e|$ , in dependence on the structure and the basis set used.<sup>24-27</sup>

For the sake of consistency, the choice of atomic charges for a model Zn-vermiculite structure was based on charge values used in the previous modelling studies of an uncharged 2:1 clay structures and obtained in quantum-chemical calculations of a clay cluster model.<sup>12,28</sup> The charges calculated on Si and Mg atoms were equal to  $+1.5642$  and  $+1.0466 |e|$ , respectively. To obtain the model structure it was supposed that the isomorphic substitution occurs only in the positions of tetrahedral atoms, whereas the octahedral positions remain fully occupied by Mg atoms. Taking into account the fact that the charge value for Al atoms should lie between the two above values, the charge of aluminium atoms was taken to be  $+1.3142 |e|$ , close to the half of the sum of the charges on the Si and Mg atoms. The difference between the charges of Si and Al atoms is equal to  $0.25 |e|$  and it is in the range of values obtained in refs. 24-27. The fact that the local environment of the Al atoms in the model clay is similar to that in zeolites justifies such a comparison. The charges on oxygen and hydrogen atoms were assumed to be the same as in the model of an uncharged 2:1 clay and the charges are equal to  $-0.7951$  and  $0.0723 |e|$ , respectively.<sup>12,28</sup>

The Zn-vermiculite model used in the calculations has  $x = 0.5$  that corresponds to 112 silicon and 16 aluminium atoms in the simulation box. To obtain the model structure, four Si atoms of each clay surface were substituted at random by aluminium atoms so that no aluminiums shared an oxygen atom (the Löwenstein rule). The presence of sixteen Al atoms in the simulation box leads to a lattice charge  $-4 |e^-|$  that is compensated by the presence of two  $\text{Zn}^{2+}$  ions in the interlayer space, one counterion per interlayer void. The chemical formula of the model structure is therefore



Hydrated Zn-vermiculite was simulated by adding 74 water molecules in each of the two interlayer voids (148 molecules in total). This water content corresponds to a water/clay mass ratio of  $218 \text{ mg g}^{-1}$  and it is in the range of experimental values for hydrated vermiculites.<sup>29,30</sup> The interlayer spacing of the structure was taken to be  $d_{001} = 14.85 \text{ \AA}$  ( $c = 29.92 \text{ \AA}$ ) and it is the same as in our previous MD study of a hydrated uncharged 2:1 clay.<sup>12</sup> This  $d_{001}$  value is in the range of interlayer distances measured for Ni-, Na-, Ca-, and Mg-vermiculites.<sup>29-31</sup> The periodic boundary conditions were applied to the simulation box in the three dimensions.

The water molecules were simulated by using a flexible SPC model.<sup>19</sup> The potential model used to describe the intermolecular water-water and water-clay interactions is the same as that used recently in ref. 12. The short-range contributions to the potential energy are represented by the sum of Lennard-Jones (12-6) potentials

$$E_{\text{LJ}} = \sum_{i=1} \sum_{j>i} \dagger 4\epsilon_{ij} \left[ \left( \frac{\sigma_{ij}}{r_{ij}} \right)^{12} - \left( \frac{\sigma_{ij}}{r_{ij}} \right)^6 \right], \quad (3)$$

where the sums run over all atoms of the system, except the counterions, and the dagger signifies the exclusion of intramolecular interactions. The values of atomic parameters  $\epsilon_{ij}$ , and  $\sigma_{ij}$  used in the calculations are presented in Table 1 and the parameters for interaction between atoms of different types were calculated from the Lorentz-Berthelot combination rule. The choice of the parameters was discussed elsewhere.<sup>12</sup>

The interactions between a  $\text{Zn}^{2+}$  ion and the oxygen and hydrogen atoms of the system were represented with the potential developed by Chillemi and co-workers<sup>18</sup> for water-zinc(II) interactions. The short-range part of the potential is written as

$$E_{\text{Zn-O}} = \frac{A_{\text{O}}}{r_{\text{ZnO}}^4} + \frac{B_{\text{O}}}{r_{\text{ZnO}}^6} + \frac{C_{\text{O}}}{r_{\text{ZnO}}^8} + \frac{D_{\text{O}}}{r_{\text{ZnO}}^{12}} E_{\text{O}} e^{-F_{\text{O}}/r_{\text{ZnO}}} \quad (4)$$

$$E_{\text{Zn-H}} = \frac{A_{\text{H}}}{r_{\text{ZnH}}^4} + \frac{B_{\text{H}}}{r_{\text{ZnH}}^6} + \frac{C_{\text{H}}}{r_{\text{ZnH}}^8}, \quad (5)$$

where  $r_{\text{ZnO}}$  and  $r_{\text{ZnH}}$  are the distances between a  $\text{Zn}^{2+}$  ion and the O and H atoms, and  $A_{\text{O}}, \dots, F_{\text{O}}, A_{\text{H}}, \dots, D_{\text{H}}$  are the parameters of the potential having numerical values reported in ref. 18. The cut-off radius ( $R_{\text{C}}$ ) of the short-range interactions was set to the half of the length of the smallest side of the simulation box  $R_{\text{C}} = 9.18 \text{ \AA}$ . The discontinuity in the energy and forces were corrected using the shifted-force technique.<sup>32</sup>

The total energy of the non-bonded interactions  $E_{\text{NB}}$  is obtained by summing the energies  $E_{\text{LJ}}$ ,  $E_{\text{Zn-O}}$ ,  $E_{\text{Zn-H}}$ , and the energy of electrostatic interactions between atoms in the system

$$E_{\text{NB}} = E_{\text{LJ}} + \sum_{\text{Zn}} \sum_{\text{O}} E_{\text{Zn-O}} + \sum_{\text{Zn}} \sum_{\text{H}} E_{\text{Zn-H}} + \sum_{i=1} \sum_{j>i} \dagger \frac{q_i q_j}{r_{ij}}, \quad (6)$$

where the sums of the second and third term run over the  $\text{Zn}^{2+}$  ions and O, and H atoms of the clay and of water molecules. The values of the atomic charges are given in Table 1. The electrostatic interactions were treated with the Ewald sum method with the parameters reported elsewhere.<sup>12</sup>

The simulation box used in calculation was built from  $4 \times 2 \times 1$  unit cells taken in the  $a$ ,  $b$ , and  $c$  crystallographic directions, respectively. The coordinates of the clay atoms were generated using the data of ref. 20 and in the simulations the atoms were kept fixed at their crystallographic positions.

**Table 1** Parameters of the Lennard-Jones potential (eqn. (3)) and values of atomic charges  $q$  used in the calculations

Atom <sup>a</sup>	$q,  e $	$\epsilon/\text{kJ mol}^{-1}$	$\sigma/\text{\AA}$
Si	+1.5642	0.397	3.951
Mg	+1.0466		
Al	+1.3142	0.272	4.112
O <sub>C</sub>	-0.7951	0.650	3.158
H <sub>C</sub>	+0.0723		
O <sub>W</sub>	-0.7890	0.650	3.158
H <sub>W</sub>	+0.3945		
Zn	+2		

<sup>a</sup> Subscripts "C" and "W" denote atoms of water molecule and clay structure, respectively.

At the beginning of the MD calculations the  $\text{Zn}^{2+}$  ions were placed in the interlayer spaces close to their midplanes. The initial mutual arrangement of the water molecules corresponded to a random distribution avoiding the overlap of van der Waals radii. Several such initial configurations were tried, all of them resulting in the same final arrangement of the species in the interlamellar space. The initial atomic velocities were chosen from a Maxwell distribution at 300 K. The classical equations of the atomic motions were integrated with the velocity form of the Verlet algorithm using a time-step of 0.4 fs. During the first 250 000 time-steps (100 ps) the system was equilibrated at the desired value of the temperature; the integration was then further performed for another 100 ps during which the coordinates and velocities of atoms were stored every eight steps (3.2 fs). This short run was used to derive information about the short-time dynamics of the interlayer species. Their long-time dynamics was studied in a much longer MD run of 2.5 ns. In this simulation, the data about positions of the counterions and atoms of the molecules were stored every 150 steps (60 fs) during the last 2.4 ns. All structural characteristics reported below were calculated using the trajectory stored during the long MD run. All simulations were performed in the  $NVT$  statistical ensemble using the weak-coupling method with a relaxation time of 0.1 ps.<sup>33</sup>

### 3 Results and discussion

#### 3.1 Structure

The adsorption of  $\text{Zn}^{2+}$  ions in water-free vermiculite takes place on the layer surfaces, in the vicinity of aluminium atoms where the electrostatic interactions are less repulsive because of the smaller positive charge of Al atoms. Upon addition of water molecules into the interlayer space cation–water complexes are built and the  $\text{Zn}^{2+}$  ions migrate to the middle plane of the space. In these complexes, the ions are surrounded by the first hydration shell consisting of six molecules and the structure of a  $\text{Zn}(\text{H}_2\text{O})_6^{2+}$  moiety in the interlamellar space does not differ from that in the aqueous solution and corresponds to a non-distorted octahedron.<sup>18,19</sup> A snapshot of the solvated  $\text{Zn}^{2+}$  ion in the interlayer space is shown in Fig. 1. Below, the twelve water molecules of the two  $\text{Zn}(\text{H}_2\text{O})_6^{2+}$  complexes and the remaining molecules will be noted as “bound” and “free” water molecules, respectively.

Fig. 2 shows the probability densities of the oxygen and hydrogen atoms of the  $\text{H}_2\text{O}$  molecules in the interlamellar space of Zn-vermiculite and compares them with those

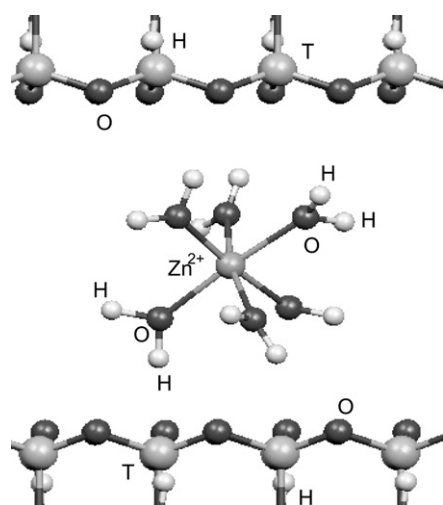


**Fig. 1** A snapshot of  $\text{Zn}(\text{H}_2\text{O})_6^{2+}$  complex in the interlamellar space of the clay structure. “T” letter stands for silicon and/or aluminium atoms of the tetrahedral sheet of clay layers.

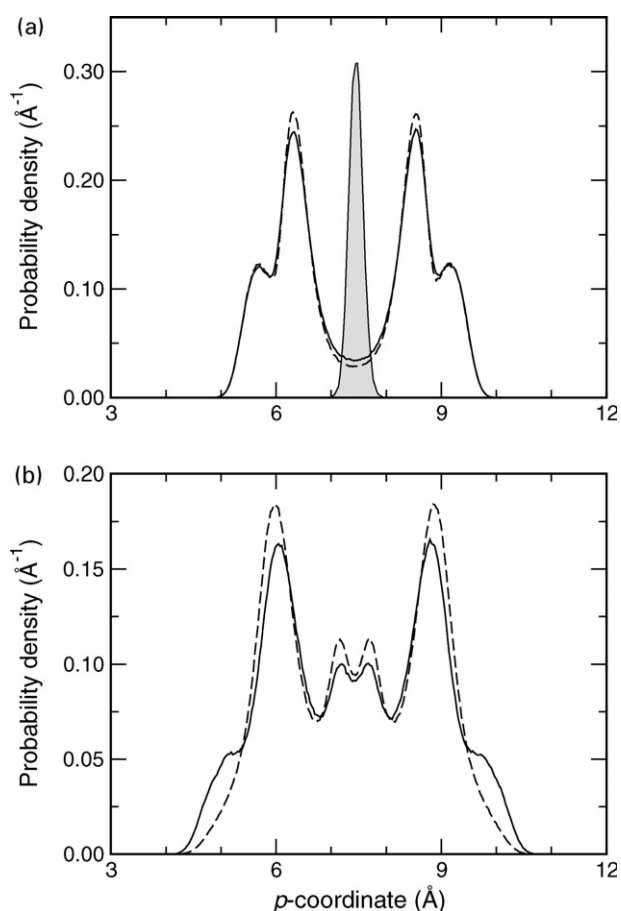


**Fig. 2** Probability densities for the oxygen (a) and hydrogen atoms (b) in Zn-vermiculite (solid line) and in an uncharged model clay structure (dashed line).<sup>12</sup> The probability density for  $\text{Zn}^{2+}$  ions is shown as a shaded contour (scaled by 0.2). The zero of the  $p$ -coordinate corresponds to the position of the Mg atoms of clay layer.

calculated for an uncharged clay.<sup>12</sup> In both structures, the water molecules form layers near the clay surfaces, each layer consisting of two sublayers, as discussed in ref. 12. In comparison with the uncharged structure, the presence of the cations in the interlayer space results in a slight increase of the probability density of the O atoms in the central part of the space, whereas the H atoms are pushed toward the surfaces, as revealed by the occurrence of well-defined peaks at *ca.* 5.1 Å and 9.9 Å (Fig. 2b). The ratio of areas of the hydrogen peaks in the water layers is calculated to be 1 : 3.9 : 1.7 that is significantly closer to the ratio 1 : 2.1 : 1.4 measured for a 14.96 Å phase  $\text{Na}^+$ -vermiculite<sup>29</sup> than the ratio 1 : 13.1 : 5.4 obtained for the cation-free structure.<sup>12</sup> The change in the relative hydrogen peak areas upon the cation introduction into the interlayer space is in good agreement with the scenario predicted in ref. 12.

Fig. 3 presents two-dimensional probability density maps  $\rho(p, \theta)$  and  $\rho(p, \phi)$ , where the angles  $\theta$  and  $\phi$  signify the angles between the molecular dipole and the  $p$  direction, and between the HH vector and the  $p$  direction, respectively. Both functions are normalized so that

$$\int_{-d_{001}}^{d_{001}} \int_0^\pi d\theta dp \rho(p, \theta) = 1 \quad \text{and} \quad \int_{-d_{001}}^{d_{001}} \int_0^{\pi/2} d\phi dp \rho(p, \phi) = 1. \quad (7)$$

The analysis of the figure shows that in the sublayer closer to the surface the molecular dipole is oriented almost parallel to the surface, while the HH vector does not reveal a preferential orientation. For the second sublayer, close to the middle plane, both the  $\rho(p, \theta)$  and  $\rho(p, \phi)$  maps display a bimodal character

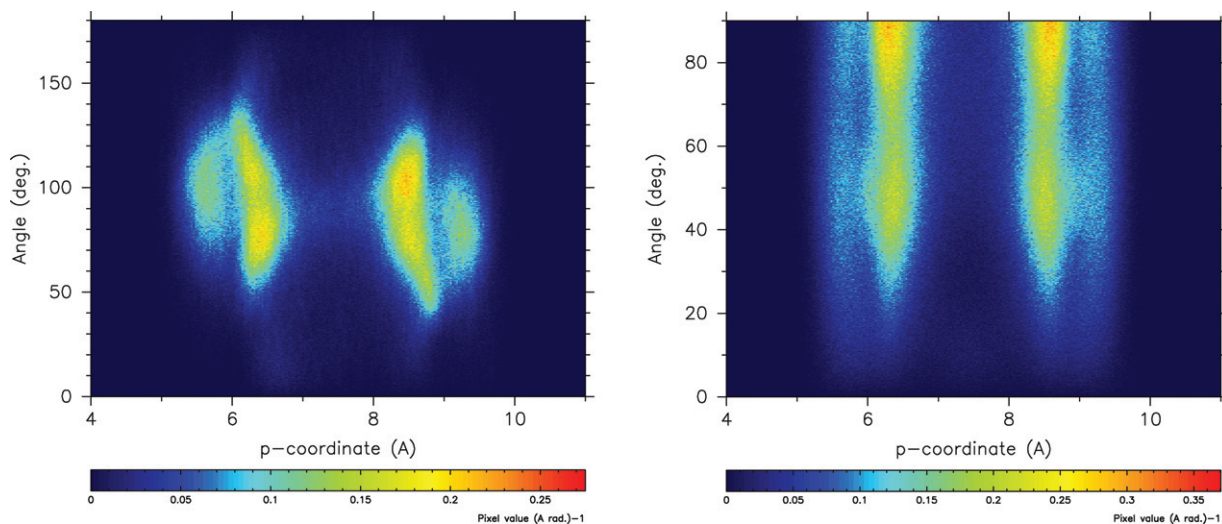


**Fig. 3** Two-dimensional probability density maps  $\rho(p,\theta)$  (left panel) and  $\rho(p,\phi)$  (right panel), see text for details. The maps for one interlayer space are shown.

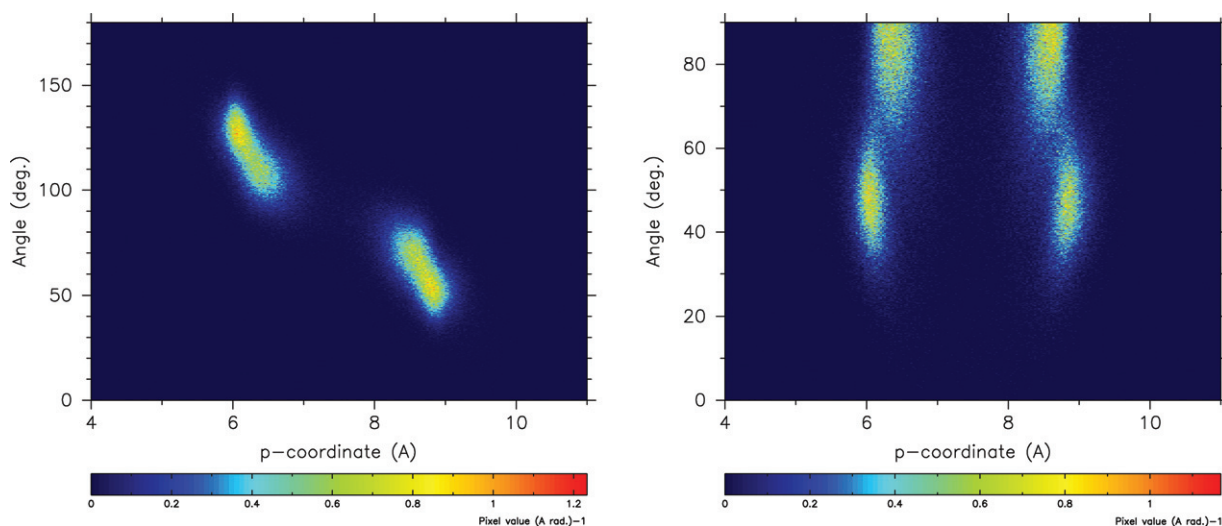
with maxima at  $\theta = 70^\circ$  and  $\theta = 110^\circ$ , and  $\phi = 90^\circ$  and  $\phi = 45^\circ$ , respectively. A wider distribution of the  $\phi$  angle, as compared to the  $\theta$  angle, indicates a less hindered motion of the HH vector of molecules than that of the molecular dipole.

Fig. 4 displays the  $\rho(p,\theta)$  and  $\rho(p,\phi)$  maps for the “bound”  $\text{H}_2\text{O}$  molecules of the Zn–water complexes and demonstrates that the molecules are not equally moved from the clay surface. The molecules which are closer to the midplane of the interlayer space have a preferential orientation with the molecular plane almost parallel to the surface, whereas the molecules in the vicinity of the surface are oriented in a way allowing hydrogen atoms of the molecules to interact with oxygen atoms of the surface (Fig. 1). Again, a wide distribution of the  $\phi$  angle, as compared to the  $\theta$  one, indicates an easier reorientation of the HH vector. Note that the maps in Fig. 3 and Fig. 4 are symmetric with respect to the midplane of the interlayer space that reflects the  $C_c$  symmetry of the clay lattice.

The results obtained can be compared with the experimental data about the structure of the cation–water complexes in vermiculites.<sup>29,30,34</sup> In all these studies the counterions were found to be located midway between the clay layers. The analysis of the hydrogen atoms profile allowed the authors to conclude that at least two third of the water molecules of the first hydration shell form hydrogen bonds to the clay surfaces. The

results of the present calculations are in good agreement with these conclusions. Indeed, both the orientation of the  $\text{Zn}(\text{H}_2\text{O})_6^{2+}$  octahedron shown in Fig. 1 and the maps presented in Fig. 4 correlate well with one of the two most probable orientations of an  $\text{M}(\text{H}_2\text{O})_6^{2+}$  complex presented in Fig. 2 of ref. 30. For the  $\text{Ni}^{2+}$ ,  $\text{Ca}^{2+}$ , and  $\text{Li}^+$  ions having the octahedral coordination in the interlayer space of vermiculites Skipper and co-workers suggested, on the basis of geometrical considerations, that the water molecules of the solvation shell form a distorted octahedron.<sup>29,30,34</sup> The results of the present calculation show that an  $\text{M}(\text{H}_2\text{O})_6^{2+}$  complex does not need to be distorted to fit the experimental data obtained by these authors. Recent Monte-Carlo and MD calculations of Mg-smectite hydrates by Greathouse *et al.*<sup>8</sup> revealed that in the interlayer space the  $\text{Mg}^{2+}$  ions form octahedral complexes with the water molecules and that the orientation of  $\text{Mg}(\text{H}_2\text{O})_6^{2+}$  is similar to that shown in Fig. 1. Each solvating water molecule was computed to form one hydrogen bond to oxygen atoms of the clay surface.

The oxygen–oxygen radial distribution function ( $g_{\text{OO}}(r)$ ) for the “free” water molecules shows that the function closely follows the  $g_{\text{OO}}(r)$  of water molecules in the uncharged clay structure.<sup>12</sup> This result indicates that at low concentrations the presence of cations in the interlamellar space modifies the



**Fig. 4** Two-dimensional probability density maps  $\rho(p,\theta)$  (left panel) and  $\rho(p,\phi)$  (right panel) for the water molecules of the first hydration shell of  $\text{Zn}^{2+}$  ions.

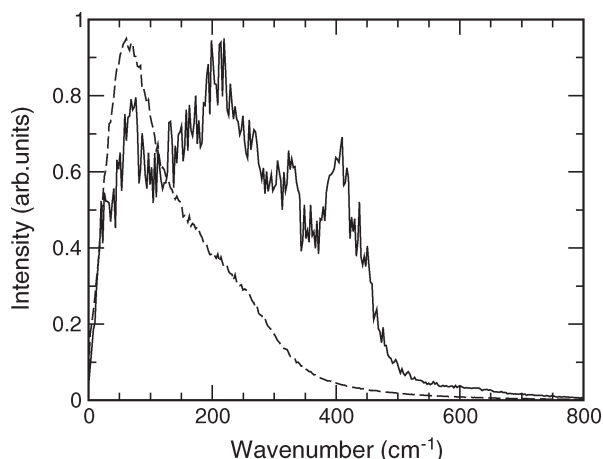
structure of the interlayer water only in the immediate vicinity of the cations.

### 3.2 Dynamical behavior of interlayer species

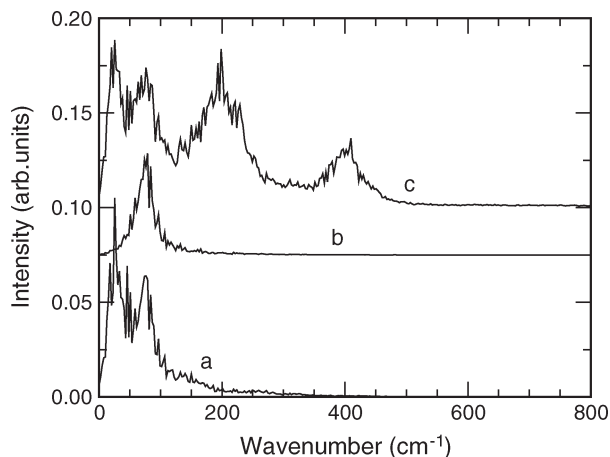
**Short-time dynamics.** Fig. 5 presents the power spectra of the molecular centers of mass (CoM) of the “free” and “bound” water. The CoM spectrum of the “free” molecules is identical to that calculated for water in the neutral clay structure.<sup>12</sup> The spectrum of “bound” water molecules reveals a complex picture of the vibrations of the molecules in a  $\text{Zn}(\text{H}_2\text{O})_6^{2+}$  complex and of the dynamics of the complex as a whole.

Fig. 6 displays the power spectra of the  $\text{Zn}^{2+}$  ion and of the CoM of the  $\text{Zn}(\text{H}_2\text{O})_6^{2+}$  octahedra. The spectra a and b in Fig. 6 show that in the interlamellar space the octahedra execute low-energy motions parallel and perpendicular (spectrum b) to the clay surfaces with frequencies of 25 and 75  $\text{cm}^{-1}$ , respectively. Therefore, the bands below 100  $\text{cm}^{-1}$  in the  $\text{Zn}^{2+}$  power spectrum (Fig. 6c) and in the CoM spectrum of the “bound” water in Fig. 5 can unambiguously be attributed to the translations of  $\text{Zn}(\text{H}_2\text{O})_6^{2+}$  complexes confined in the interlayer void. Bands in the region above 100  $\text{cm}^{-1}$  then belong to the internal dynamics of the  $\text{Zn}(\text{II})$ -water complexes. The previous MD study of  $\text{Zn}^{2+}$  in aqueous solution permitted to assign the bands at 200 and 400  $\text{cm}^{-1}$  in the  $\text{Zn}^{2+}$  power spectrum to the  $\omega_5$  and  $\omega_6$  modes, respectively, following the classification by Kohlrausch.<sup>35</sup> These modes involve a displacement of the zinc ion, while four other modes of the octahedron, in which  $\text{Zn}^{2+}$  remains at rest, do not give rise to a signal in the spectrum of the cation but are expected in the region 100–400  $\text{cm}^{-1}$  of the CoM spectrum of the “bound” molecules<sup>19</sup> (Fig. 5). The comparison of the spectra of the confined  $\text{Zn}(\text{H}_2\text{O})_6^{2+}$  complex with those in aqueous solution reveals no noticeable difference, thus suggesting that the confinement does not change the internal dynamics of the complexes. This result agrees with the finding that the structure of the octahedron formed by six water molecules of the first solvation shell is the same in the interlayer space of the clay and in the solution.

The rotational dynamics of the “bound” water molecules mostly involves changes of orientation of the HH vector with the orientational relaxation time  $\tau_{\text{HH}} = 10.8$  ps, while the molecular dipole of the molecules hardly changes its orientation and this motion is characterized by a relaxation time of at least one order of magnitude larger than that of the HH vector. The rotational dynamics of the “free” water in Zn-vermiculite structure gives rise to the orientational relaxation times of the HH vector and of the molecular dipole  $\tau_{\text{HH}} = 3.3$  ps and  $\tau_{\mu} = 9.5$  ps, respectively. The relaxation time calculated



**Fig. 5** Center of mass power spectra of “bound” (solid line) and “free” (dashed line) water molecules in Zn-vermiculite.



**Fig. 6** Power spectrum of the CoM of  $\text{Zn}(\text{H}_2\text{O})_6^{2+}$  octahedra (a), the CoM spectrum with the polarization perpendicular to the surface (b), and power spectrum of  $\text{Zn}^{2+}$  ions (c) in the Zn-vermiculite structure.

for the molecular dipole is markedly larger than that in the neutral clay structure ( $\tau_{\mu} = 6.8$  ps).<sup>12</sup> The increase of the dipole orientational relaxation time in the presence of  $\text{Zn}^{2+}$  ions can find its origin in a damping of the dipole reorientations due to the interaction with the spatially fixed molecular dipoles of the “bound” molecules of the zinc-water complexes. Such stiffness of the dipole orientation should be more pronounced at higher concentrations of counterions.

The relaxation time for the HH vector is close to that calculated for  $\text{H}_2\text{O}$  molecules in the uncharged structure  $\tau_{\text{HH}} = 3.6$  ps;<sup>12</sup> note that both values are not very different from the relaxation time  $\tau_{\text{HH}} = 2.3$  ps for molecules in bulk water.<sup>19</sup> The value of  $\tau_{\text{HH}}$  relaxation time, as well as the trends obtained, are in good agreement with the recent femtosecond pump-probe spectroscopic measurements<sup>37</sup> which showed that the orientational relaxation time of water molecules in aqueous solution of a strong structure maker such as  $\text{Mg}^{2+}$  ion ( $\tau_{\text{or}} = 3.2 \pm 0.2$  ps) does not differ significantly from the value in bulk water ( $\tau_{\text{or}} = 2.5 \pm 0.1$  ps).

**Residence times.** As in aqueous solution, the water molecules of the  $\text{Zn}(\text{H}_2\text{O})_6^{2+}$  complexes in the interlamellar space form a stable octahedral environment of the ions with a residence time in the first solvation shell longer than the length of the 2.4 ns simulation run. In contrast, the second hydration shell of  $\text{Zn}^{2+}$  ions is much less stable. The residence time of molecules in the second hydration shell were computed with the use of the Impey method<sup>36</sup> from an exponential fit of a “survival function”  $n(t)$  that defines the number of molecules remaining in the shell after time  $t$  as

$$n(t) = \frac{1}{N_T} \sum_{i=1}^{N_T} \sum_{m=1}^{N_M} P_m(t, t_i, t^*). \quad (8)$$

In eqn. (8) the index  $i$  runs over  $N_T$  time origins and the binary function  $P_m(t, t_i, t^*)$  is equal to 1 if the molecule  $m$  belongs to the hydration shell at both time  $t_i$  and  $t_i + t$  and does not leave the shell during that interval for a period longer than  $t^*$ , and it is 0 otherwise. The calculations were carried out using the “return time”  $t^*$  equal to 0.16 ps that corresponds to the vibrational period of the center of mass of H-bonded water molecules.

The second hydration shell of the zinc ions in the Zn-vermiculite structure is built of 9.2  $\text{H}_2\text{O}$  molecules as compared with 12.5 molecules in solution.<sup>19</sup> The decrease of the number of molecules in the second hydration shell is obviously due to the confinement; the lack of molecules in the shell is compensated by H-bonds of the solvating molecules with the oxygen

atoms of the clay surfaces. For the H<sub>2</sub>O molecules of the second shell of the ions in the interlayer space the calculations yield the residence time of  $28.4 \pm 1.2$  ps. This value is four times larger than the residence time of 7.3 ps computed for molecules of the second hydration shell of Zn<sup>2+</sup> in aqueous solution.<sup>19</sup> Anticipating section 3.3, the present results show that the diffusion coefficient of the “free” interlayer water is about four times smaller than in the liquid water. The ratio of the residence times in the ionic solution and in the clay structure then corresponds to the ratio of the diffusion coefficients of water molecules in bulk water and in the Zn-vermiculite structure. This result indicates that the increase of the residence time of the water molecules in the second hydration shell of the ions is due to the confinement in the interlayer space but not to a modification of the intermolecular interactions due to the presence of cations.

The long lifetime of the “bound” water molecules in the hydration shell agrees with the residence time  $> 10^{-8}$  s obtained from EXAFS measurements of Zn<sup>2+</sup> aqueous solution<sup>38</sup> that is by one order of magnitude longer than the length of the MD run. The present results are also in line with the data of quasi-elastic neutron scattering studies by Tuck and co-workers of Ca<sup>2+</sup>-montmorillonite and Ca<sup>2+</sup>-, Mg<sup>2+</sup>- and Na<sup>+</sup>-vermiculites.<sup>39,40</sup> Using spectrometers of different resolution the authors showed that any exchange between the water molecules of the first hydration shell and the “free” water molecules can only happen in the time-scale longer than  $10^{-10}$  s. Indeed, Greathouse and co-workers<sup>8</sup> observed an exchange between the molecules of the first hydration shell of the Mg<sup>2+</sup> ions and the “free” water molecules in the Mg-smectite in their MD calculations covering 1175 ps period; the process was observed neither experimentally nor in the present calculations.

### 3.3 Single-particle dynamics of interlayer water

Fig. 7 shows the trajectories of “bound” and “free” H<sub>2</sub>O molecules in the *ab* crystallographic plane during the 2.4 ns MD run. The translational motion of the “bound” water is limited to a relatively small region. Such a spatially restricted motion is obviously due to the interaction of the Zn(H<sub>2</sub>O)<sub>6</sub><sup>2+</sup> complex with the clay surface. The complex is engaged with the surface oxygen atoms by H atoms of the solvating molecules and these interactions significantly limit the mobility of

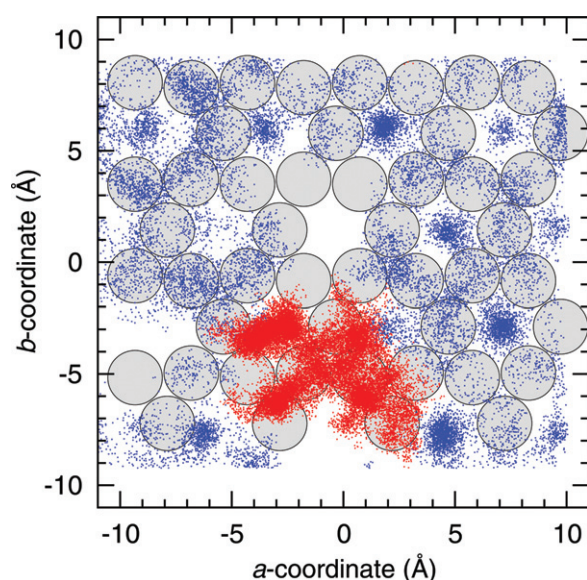


**Fig. 7** CoM trajectory of a “bound” molecule (red) and a “free” molecule (blue) in the *ab* crystallographic plane in the 2.4 ns MD run. The large grey circles denote oxygen atoms of the clay surface.

the complex. In contrast, the “free” water molecule explores almost all the available space although Fig. 7 reveals the existence of preferred adsorption positions, which were discussed in ref. 12 in details. Note that for both types of water the motion parallel to the surface has significantly larger amplitudes than in the *p*-direction (Fig. 2).

The single-particle dynamics of the interlayer water was investigated by the analysis of the intermediate scattering functions (ISCFs). The time Fourier transform of the intermediate scattering function gives the dynamic structure factor  $S(\mathbf{Q}, \omega)$  that is measured by quasi-elastic neutron scattering (QENS) spectroscopy.<sup>41</sup> The  $I(\mathbf{Q}, t)$  function is calculated as

$$I(\mathbf{Q}, t) = \sum_i b_i^2 \langle \exp(i\mathbf{Q}(\mathbf{r}_i(t) - \mathbf{r}_i(0))) \rangle, \quad (9)$$

where  $\mathbf{Q} = \mathbf{k}_0 - \mathbf{k}$  is the vector of the momentum transfer with  $\mathbf{k}_0$  and  $\mathbf{k}$  being the momenta of the incident and scattered neutrons, and the angle brackets denote an average over the statistical ensemble. The index *i* in eqn. (9) runs over the atoms of the water molecules, and the atomic contributions are weighted by the incoherent scattering cross-section  $b_i^2$  of atoms. With the cross-section of hydrogen being several order of magnitude larger than the incoherent cross-section of oxygen atom,<sup>42</sup> the ISCFs principally contain the information about the dynamics of the H atoms.

Taking into account the fact that the diffusional motion of the water molecules has essentially a two-dimensional character, in the calculations of the ISCFs the vector of momentum transfer was directed parallel to the surface of the clay layers (in the *ab* crystallographic plane). Assuming an isotropic motion in the plane the vector notation for the momentum transfer  $\mathbf{Q}$  is hereafter replaced by its absolute value  $Q$ . The calculations of the ISC functions were carried out for the “free” H<sub>2</sub>O molecules only, since the small number of “bound” water molecules limits the reliability of calculated ISCFs and of the subsequent analysis.

Fig. 8 presents the intermediate scattering functions calculated for two values of the momentum transfer. In the time interval  $t > 1$  ps, where the contribution from the rotational motion is expected to be negligible, the functions were approximated with the Kohlrausch–Williams–Watts (KWW) stretched-exponential function  $\phi_{\text{KWW}}(t)$

$$\phi_{\text{KWW}}(t) = A \exp(-(t/\tau)^\beta) + B, \quad (10)$$

where *A*, *B*,  $\tau$ , and  $\beta$  are parameters;  $\tau$  and  $\beta$  being the relaxation and the stretching parameter, respectively. The mean relaxation time  $\langle \tau \rangle$  is obtained from the parameters as

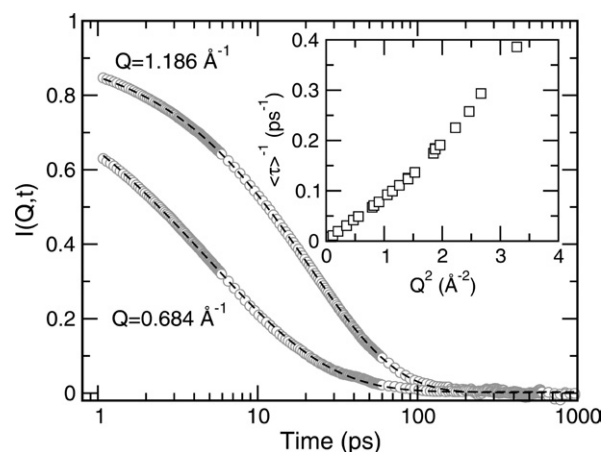


**Fig. 8** Intermediate scattering functions (eqn. (9)) calculated for the “free” water molecules. The dashed lines show the fit of the ISCFs by KWW function (eqn. (10)). The inset presents a plot of  $\langle \tau \rangle^{-1}$  against the square of momentum transfer  $Q$  (see text for details).

$\langle\tau\rangle = \tau/\beta \Gamma(1/\beta)$ , where  $\Gamma(x)$  is the Gamma function. In the limit of small  $Q$  values (large distances), the diffusion coefficient  $D$  can be obtained from the relation  $\langle\tau\rangle = 1/(DQ^2)$ . The calculated dependence of the inverse mean relaxation time  $\langle\tau\rangle^{-1}$  on the square of momentum transfer is shown in the inset in Fig. 8. The fitting by a linear function in the region of  $Q^2 < 1.5 \text{ \AA}^{-2}$  results in the diffusion coefficient  $D = (0.89 \pm 0.01) \times 10^{-9} \text{ m}^2 \text{ s}^{-1}$  that is close to the diffusion coefficient  $(0.94 \pm 0.02) \times 10^{-9} \text{ m}^2 \text{ s}^{-1}$  obtained in the same way for water molecules in the uncharged clay.<sup>12</sup>

Experimentally, the information about the single-particle dynamics of interlayer water is derived from the analysis of the quasi-elastic broadening of the elastic peak in the neutron scattering experiments. Fig. 9 presents the dynamic structure factor  $S(Q, \omega)$  calculated for two values of the momentum transfer. Following the commonly accepted procedure, the  $S(Q, \omega)$  spectra were fitted by a Lorentzian function<sup>43</sup> and a plot of the half-width at half maximum  $\Delta\omega$  of the functions against  $Q^2$  is shown in the inset in Fig. 9. If the diffusion of the molecules in the interlamellar space would follow the continuous diffusion model, the dependence would be a straight line with the slope proportional to the diffusion coefficient. The dependence  $\Delta\omega(Q^2)$  shown in Fig. 9 clearly deviates from the straight line at large  $Q$  values and the obtained dependence can be fitted with the two-dimensional jump-diffusion model<sup>12,44</sup>

$$\Delta\omega(Q) = \frac{\hbar}{\tau_{\text{res}}} [1 - \exp(-Q^2 \langle r^2 \rangle / 4)], \quad (11)$$

where  $\tau_{\text{res}}$  is the mean residence time and  $\langle r^2 \rangle$  stands for the mean square jump length. The fitting results in the parameters values  $\tau_{\text{res}} = 7.27 \pm 0.39 \text{ ps}$  and  $\langle r^2 \rangle = 2.64 \pm 0.26 \text{ \AA}^2$  which yield the diffusion coefficient  $D = \langle r^2 \rangle / 4\tau_{\text{res}} = (0.91 \pm 0.11) \times 10^{-9} \text{ m}^2 \text{ s}^{-1}$ . Within the uncertainty limits, the parameters and thus the resulting coefficient coincide with those calculated for water in the model structure of uncharged clay.<sup>12</sup> Thus, the presented analysis shows that the single-particle dynamics of the “free” water molecules in the  $\text{Zn}^{2+}$ -vermiculite structure at low concentration of the cations is not significantly influenced by the presence of cations. The diffusion coefficient calculated for the interlayer water is four times smaller than the coefficient obtained for the liquid water.<sup>19</sup>

The quasi-elastic neutron scattering studies by Tuck *et al.*<sup>39,40</sup> showed that the non-bound water molecules in  $\text{Ca}^{2+}$  exchanged montmorillonites and vermiculites undergo a diffusional motion with a diffusion coefficient in the range  $0.02\text{--}1.13 \times 10^{-9} \text{ m}^2 \text{ s}^{-1}$ , in dependence on the water-vapour relative

pressure and on the clay structure. The lowest values of the diffusion coefficient were obtained for small relative pressures, where only a small number of the non-coordinated water molecules in the interlamellar space is expected, and for vermiculite clays which have a higher cation exchange capacity than montmorillonites. The diffusion of the non-coordinated molecules was suggested to occur *via* jumps between cages formed by the hydrated cations<sup>40</sup> with a mean distance between the cages estimated to be between 3 and 4  $\text{\AA}$ . In the case of the present study, such a distance, which corresponds to the distance between one  $\text{Zn}(\text{H}_2\text{O})_6^{2+}$  complex and its image generated by the periodic boundary conditions in the *ab* plane, is at least four times larger. More recently, the QENS experiments by Swenson and co-workers<sup>45</sup> performed on  $\text{Na}^+$ -vermiculite structure showed that some of the confined  $\text{H}_2\text{O}$  molecules have the diffusion coefficient  $D = 0.88 \times 10^{-9} \text{ m}^2 \text{ s}^{-1}$  that is close to the values obtained in the present calculations. These water molecules were suggested to correspond to the “free” water molecules of the present calculations. The recent neutron resonance spin-echo measurements, which covered the 3–3000 ps time interval of the ISC function and carried out for the same system,<sup>46,47</sup> revealed the existence of a slower dynamics of the confined water and this motion was attributed to the molecules involved in the first hydration shell of the cations.

In the MD calculations of Mg-beidelite, Greathouse *et al.*<sup>8</sup> obtained the diffusion coefficient of water molecules  $D = 0.199\text{--}0.248 \times 10^{-9} \text{ m}^2 \text{ s}^{-1}$  that falls in the range of experimentally measured values.<sup>39,40</sup> Molecular dynamics studies of  $\text{Li}^+$  and  $\text{Na}^+$  montmorillonite hydrates<sup>6</sup> resulted in the diffusion coefficients of the interlayer water  $D = 0.45 \times 10^{-9}$  and  $D = 0.79 \times 10^{-9} \text{ m}^2 \text{ s}^{-1}$ , respectively. Note that the water molecules of the first solvation shell were included in the calculation of mean-square atomic displacements used to obtain the coefficients *via* the Einstein relationship. Such a procedure should lead to a smaller value of the effective diffusion coefficient as the solvating molecules are less movable.

Comparing results of the present study with the data of the previous experimental and modelling works one can conclude that the diffusion coefficient calculated for non-solvating water in the Zn-vermiculite structure has an absolute value comparable with the values obtained from those studies. Surprisingly, the presence of the cations in the interlamellar space does not significantly modify the mobility of the water molecules. This conclusion agrees with the other results of the present calculations about the structure and the short-time dynamics of the interlayer water.

## 4 Conclusions

The structure and dynamics of the interlayer species in hydrated Zn-vermiculite structure were studied in details by means of molecular dynamics simulation technique. The calculations were carried out at  $T = 300 \text{ K}$  and for a low concentration of the counterions in the interlayer space. In a water-free structure the counterions are adsorbed on the surface of clay layers, near aluminium atoms. The introduction of  $\text{H}_2\text{O}$  molecules into the interlayer space leads to the formation of zinc-water complexes that is accompanied by the migration of the  $\text{Zn}^{2+}$  ions towards the midplane of the interlayer space. The complex consists of six water molecules forming an octahedron with the cation in the center of the octahedron. The  $\text{Zn}(\text{H}_2\text{O})_6^{2+}$  complexes in the interlayer space are oriented so that at least four water molecules interact *via* their hydrogen atoms with the oxygen atoms of the clay surfaces. Due to the confinement the translational dynamics of the complex is anisotropic.

The calculations show that in the interlamellar space the Zn-water complexes have the same structure and internal dynamics as in aqueous solution.<sup>19</sup> The rotational motion of

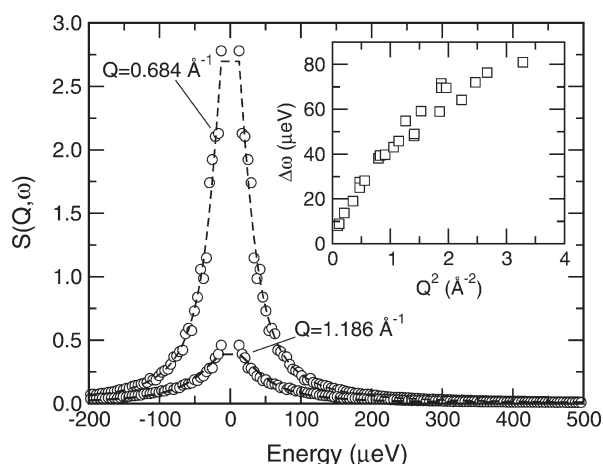


**Fig. 9** Dynamic structure factors  $S(Q, \omega)$  calculated for the same values of  $Q$  as in Fig. 8. The dashed lines show the fit of the  $S(Q, \omega)$  by Lorentzian functions. The inset displays a plot of the half-width at half maximum of the Lorentzian functions against the square of momentum transfer  $Q$ .

both the “bound” and “free” molecules proceeds mostly *via* a reorientation of the HH vector of the molecules. For “free” water molecules, the orientational relaxation time does not significantly differ from that in the liquid water and in the neutral clay structure.<sup>12</sup> No exchange between the solvating water molecules and the “free” water of the interlayer space was observed in the time-scale of the present calculations (2.4 ns). The residence of H<sub>2</sub>O molecules in the second hydration sphere of the cations was computed to be of *ca.* 28 ps that is approximately four times longer than that in aqueous solution. The increase of the residence time corresponds to the decrease of the diffusion coefficient of the interlayer water, as compared to the molecules in the liquid.

The calculation shows the spatially restricted translational dynamics of the “bound” molecules in the *ab* crystallographic plane, whereas the “free” water moves relatively easily. The single-particle dynamics of the non-solvating water molecules was studied by the analysis of the intermediate scattering functions and by calculation of the quasi-elastic neutron scattering spectra. The resulting diffusion coefficients of the “free” water as well as parameters of the jump-diffusion model used to analyze the QENS spectra,<sup>12,44</sup> were calculated to be very close to those of the H<sub>2</sub>O molecules in the uncharged clay.<sup>12</sup> The diffusion coefficient  $D = (0.91 \pm 0.11) \times 10^{-9} \text{ m}^2 \text{ s}^{-1}$  is four times smaller than that in liquid water.

The results obtained show that the presence of the cations in the interlayer space modify neither structure nor dynamics of the “free” water molecules. This conclusion agrees with the opinion that the role of the clay surfaces and of the hydrated cations is mainly to enforce spatial restrictions on the dynamics of the “free” water molecules.<sup>39</sup> It also correlates with the results of recent experiments which suggest that an aqueous salt solution can be viewed as a colloidal suspension of inert particles, formed by the ions plus their first hydration shell, in a pure liquid water.<sup>37</sup> We, however, stress that some of the results of the present calculations might be influenced by the increase of the concentration of the counterions in the interlamellar space. Indeed, the Zn<sup>2+</sup> concentration used is roughly eight times lower than the concentrations of divalent ions in the experimental studies.<sup>29,30,34,45</sup> The influence of the concentration, the temperature as well as of the interlayer spacing on the behavior of the confined species will be the subject of future modelling studies.

## Acknowledgements

M. A. gratefully acknowledges a Fellowship from the “Centre National de la Recherche Scientifique” and from the “Région Nord-Pas de Calais”. This work is a part of the “Programme de Recherche Concerté: Sites et Sols Pollués” supported by the “Région Nord-Pas de Calais” and the “Fonds Européen de Développement Economique des Régions” (FEDER). The authors thank the project “Calcul Intensif” at USTL for the allocation of computing resources.

## References

- 1 W. N. Lipscomb and N. Sträter, *Chem. Rev.*, 1996, **96**, 2375.
- 2 D. R. Roberts, A. C. Scheinost and D. L. Sparks, *Environ. Sci. Technol.*, 2002, **36**, 1742.
- 3 N. T. Skipper, F.-R. Chou Chang and G. Sposito, *Clays Clay Miner.*, 1995, **43**, 285.
- 4 N. T. Skipper, G. Sposito and F.-R. Chou Chang, *Clays Clay Miner.*, 1995, **43**, 294.
- 5 E. S. Boek, P. V. Coveney and N. T. Skipper, *J. Am. Chem. Soc.*, 1995, **117**, 12608.
- 6 F.-R. Chou Chang, N. T. Skipper and G. Sposito, *Langmuir*, 1997, **13**, 2074.

- 7 K. S. Smirnov and D. Bougeard, *J. Phys. Chem. B*, 1999, **103**, 5266.
- 8 J. A. Greathouse, K. Refson and G. Sposito, *J. Am. Chem. Soc.*, 2000, **122**, 11459.
- 9 D. A. Young and D. E. Smith, *J. Phys. Chem. B*, 2000, **104**, 9163.
- 10 E. J. M. Hensen, T. J. Tambach, A. Bliëk and B. Smit, *J. Chem. Phys.*, 2001, **115**, 3322.
- 11 E. J. M. Hensen and B. Smit, *J. Phys. Chem. B*, 2002, **106**, 12664.
- 12 M. Arab, D. Bougeard and K. S. Smirnov, *Phys. Chem. Chem. Phys.*, 2003, **5**, 4699.
- 13 T. S. Hofer, H. T. Tran, C. F. Schwenk and B. M. Rode, *J. Comput. Chem.*, 2003, **25**, 211, and references cited therein.
- 14 E. Clementi, G. Corongiu, B. Jönsson and S. Romano, *J. Chem. Phys.*, 1980, **72**, 260.
- 15 Y. P. Yongyai, S. Kokpol and B. M. Rode, *Chem. Phys.*, 1991, **156**, 403.
- 16 G. W. Marini, N. R. Texler and B. M. Rode, *J. Phys. Chem.*, 1996, **100**, 6808.
- 17 J. M. Martínez, R. R. Pappalardo and E. S. Marcos, *J. Phys. Chem.*, 1993, **97**, 4500.
- 18 G. Chillemi, P. D’Angelo, N. Viorel Pavel, N. Sanna and V. Barone, *J. Am. Chem. Soc.*, 2002, **124**, 1968.
- 19 M. Arab, D. Bougeard and K. S. Smirnov, *Chem. Phys. Lett.*, 2003, **379**, 268.
- 20 A. McL. Mathieson and G. F. Walker, *Am. Mineral.*, 1954, **39**, 231.
- 21 D. Tunega, G. Haberhauer, M. H. Gerzabek and H. Lischka, *Langmuir*, 2002, **18**, 139.
- 22 A. Delville, *Langmuir*, 1992, **8**, 1796.
- 23 A. Chatterjee, T. Iwasaki, T. Ebina and H. Hayashi, *Appl. Surf. Sci.*, 1997, **121/122**, 167.
- 24 A. C. Hess and V. R. Saunders, *J. Phys. Chem.*, 1992, **96**, 4367.
- 25 J. L. Anchell, J. C. White, M. R. Thompson and A. C. Hess, *J. Phys. Chem.*, 1994, **98**, 4463.
- 26 J. C. White, J. B. Nicholas and A. C. Hess, *J. Phys. Chem.*, 1997, **101**, 590.
- 27 J. B. Nicholas and A. C. Hess, *J. Am. Chem. Soc.*, 1994, **116**, 5428.
- 28 M. Arab, D. Bougeard and K. S. Smirnov, *Phys. Chem. Chem. Phys.*, 2002, **4**, 1957.
- 29 N. T. Skipper, A. K. Soper and J. D. C. McConnell, *J. Chem. Phys.*, 1991, **94**, 5751.
- 30 N. T. Skipper, A. K. Soper and M. V. Smalley, *J. Phys. Chem.*, 1994, **98**, 942.
- 31 A. V. de Siqueira, C. Lobban, N. T. Skipper, G. D. Williams, A. K. Soper, R. Done, J. W. Dreyer, R. J. Humphreys and J. A. R. Bones, *J. Phys.: Condens. Matter*, 1999, **11**, 9179.
- 32 M. P. Allen, D. Tildesley, *Computer Simulation of Liquids*, Clarendon Press, Oxford, 1987.
- 33 H. J. C. Berendsen, J. P. M. Postma, W. F. van Gunsteren, A. DiNola and J. R. Haak, *J. Chem. Phys.*, 1984, **81**, 3684.
- 34 N. T. Skipper, M. V. Smalley, G. D. Williams, A. K. Soper and C. H. Thompson, *J. Phys. Chem.*, 1995, **99**, 14201.
- 35 K. W. F. Kohlrausch, *Ramanspektren*, Heyden & Son Ltd., New York, 1943, p. 166.
- 36 R. W. Impey, P. A. Madden and I. R. McDonald, *J. Phys. Chem.*, 1983, **87**, 5071.
- 37 A. W. Omta, M. F. Kropman, S. Woutersen and H. J. Bakker, *J. Chem. Phys.*, 2003, **119**, 12457.
- 38 T. Miyazawa, Y. Sawa, Y. Sakane and I. Watanabe, *Physica B: Condens. Matter*, 1995, **208–209**, 393.
- 39 J. J. Tuck, P. L. Hall, M. H. B. Hayes, D. K. Ross and C. Poinsignon, *J. Chem. Soc., Faraday Trans. 1*, 1984, **80**, 309.
- 40 J. J. Tuck, P. L. Hall, M. H. B. Hayes, D. K. Ross and J. B. Hayter, *J. Chem. Soc., Faraday Trans. 1*, 1985, **81**, 833.
- 41 M. Bée, *Quasielastic Neutron Scattering: Principles and Applications in Solid State Chemistry, Biology and Materials Science*, Adam Hilger, Bristol, 1988, ch. 2.
- 42 B. S. Hudson, *J. Phys. Chem. A*, 2001, **105**, 3949.
- 43 Due to the finite length of the calculated ISCFs the values of  $S(Q, \omega)$  near  $\omega = 0$  are subject to large errors. Therefore, the five points of  $S(Q, \omega)$  in the range  $[-2\delta\omega; +2\delta\omega]$ , where  $\delta\omega = 4.21 \mu\text{eV}$  is the energy-step in the calculated spectra, were excluded from the analysis.
- 44 P. L. Hall and D. K. Ross, *Mol. Phys.*, 1981, **42**, 673.
- 45 J. Swenson, R. Bergman and W. S. Howells, *J. Chem. Phys.*, 2000, **113**, 2873.
- 46 J. Swenson, R. Bergman, S. Longeville and W. S. Howells, *Physica B*, 2001, **301**, 28.
- 47 J. Swenson, R. Bergman, D. T. Bowron and S. Longeville, *Philos. Mag. B*, 2002, **82**, 497.